

## The Relationship between the Meridional Profile of Zonal-mean Geostrophic Wind and Station Wave at 500 hPa<sup>①</sup>

Fang Zhifang (方之芳)

*Chengdu University of Information Technology, Chengdu 610041*

John M. Wallace and David W. J. Thompson

*Department of Atmospheric Sciences, University of Washington, Seattle, U.S.A*

(Received September 1, 2000)

### ABSTRACT

The sea-level pressure (SLP), 500 hPa height, zonal-mean 500 hPa height ( $Z_{500}$ ), stationary wave eddy component of the 500 hPa height ( $Z_{500}^*$ ) and zonal-mean 500 hPa geostrophic wind [ $U_z$ ] fields poleward of 20°N are examined for the period 1958–1997, with emphasis on the winter season. The relationships between the Arctic Oscillation (AO) index and algebraic difference of the zonal-mean wind in 55°N and 35°N (Ut) index were investigated, making use the Monte Carlo procedure, Singular Value Decomposition (SVD), Empirical orthogonal function (EOF) and regression method. The leading modes of empirical orthogonal function (EOF's) of SLP are more robust than the 500 hPa height EOF's, not only in the ratio of the two largest eigenvalues, but in more zonally symmetric. Comparing the meridional profiles of zonal-mean wind amplitude associated with the AO and Ut index, the profiles for the two indexes are very similar, both with respect to amplitude and the placement of the maximum and minimum. Comparing the station wave component of 500 hPa height field regressed upon the AO and Ut index, there is one-to-one correspondence between all the major centers of action in the two maps, especially in the North Atlantic and Eurasian continent. The pattern is unlike the prominent teleconnection patterns, they have hemispheric extent and cannot be interpreted in term of the individual wavetrains.

**Key words:** Meridional profile, Station wave, Eddy component, Zonal-mean geostrophic wind, Arctic Oscillation

### 1. Introduction

The empirical orthogonal function (EOF) method is applied widely in analyzing the atmospheric pattern in 500 hPa height field and sea level pressure field. In the Northern Hemisphere wintertime monthly mean 500 hPa height field, the ratio of the two largest eigenvalues is 1.4 (Cheng, et al. 1995). In contrast, the ratio of the two leading eigenvalues of the sea level pressure (SLP) field is 2 (Thompson and Wallace, 1998, 2000). The corresponding EOF1 pattern of SLP is highly reproducible than 500 hPa. They have labeled the leading pattern of the monthly mean sea level pressure anomaly field as "the Arctic Oscillation".

Ting et al. (1996) had documented that the three-dimensional structures of the stationary wave respond to a distinctive mode of variability of the zonally averaged basic state. A meridional seasaw in zonal momentum was represented by the algebraic difference of the zonal-mean wind between 55°N and 35°N, hereafter referred to as "index of Ting" or "Ut".

<sup>①</sup>This work was supported by LASG, Institute of Atmospheric Physics, Chinese Academy of Sciences in 2000 and the National Science Foundation of U.S.A. under Grant No. 9805886.

This particular choice of index was motivated by statistics derived from a suite of experiments with a linear baroclinic stationary wave model and prior analyses of observational data by Branstator (1984) and Kidson (1985).

The purpose of this paper is to show that the EOF's of SLP are more robust than the 500 hPa height EOF's, not only in the ratio of the two largest eigenvalues, but in more zonally symmetric. In order to more clearly elucidate the relationships between the AO and Ut index, we compare the meridional profiles of zonal-mean wind amplitude associated with the AO and Ut index, and the station wave component of 500 hPa height field regressed upon the AO and Ut index. We investigated a new pattern in the Northern Hemisphere. To identify the pattern, we make use of the SVD, EOF and regression method. The analysis is restricted to the winter season, when the relationships are the strongest.

## 2. Dataset and methods

The analysis described in this paper is based on the data set: Monthly mean atmospheric 500 hPa height and sea-level pressure anomaly fields poleward of 20°N, derived from the NCEP/NCAR reanalyses data for the winter months (DJF), beginning with Jan. 1958 and ending with Feb. 1997. The  $2.5^\circ \times 2.5^\circ$  lat-long grid data were weighted by the square root of cosine of latitude.

Based on the work of Thompson and Wallace (1998, 2000), the leading principal component (PC1) of the sea-level pressure anomaly field was defined as the Arctic Oscillation index, hereafter referred to as AO index. The leading pattern of the sea-level pressure was defined as "the Arctic Oscillation" or AO mode.

## 3. Results

### 3.1 Comparison between the leading mode of SLP and 500 hPa height

The leading modes of 500 hPa height and SLP field based on 119 months are shown in Fig. 1. The ratios of the two largest eigenvalues in 500 hPa and SLP are 1.33 and 1.94, they are similar to the results by Cheng et al. (1995) and Thompson and Wallace (1998). In accordance with the definition, the leading SLP mode (Fig. 1a) is corresponding to the AO mode. It bears a resemblance to the NAO pattern, but its primary center was covered on the Arctic Ocean, giving it a more zonally symmetric appearance than 500 hPa. It can be interpreted as the surface signature of modulations in the strength of the polar vortex aloft, published by Thomson and Wallace (1998). Though its 500 hPa counterpart (Fig. 1b) is somewhat different from SLP mode in structure, but there exists a strong correlation coefficient (0.88) between their respective PC1 time series. It strongly resembles the pattern that was obtained by regressing the 500 hPa height field upon the AO index by Thomson and Wallace (1998). In both 500 hPa height and the SLP fields, the second mode was dominated by the Pacific sector which exhibits the familiar signature of the PNA pattern by Wallace and Gutzler (1981) (figure omitted).

The correlation coefficient field map between the SLP and 500 hPa is shown in Fig. 2. Because of barotropic conditions over the ocean, the higher correlation coefficients areas appeared in the Pacific and the Atlantic, the values are more than 0.90 in large extent, and practically all correlation coefficients are positive values. But there exist two lower correlation coefficient areas in the Eurasian and North American continent, which was influenced by the land.

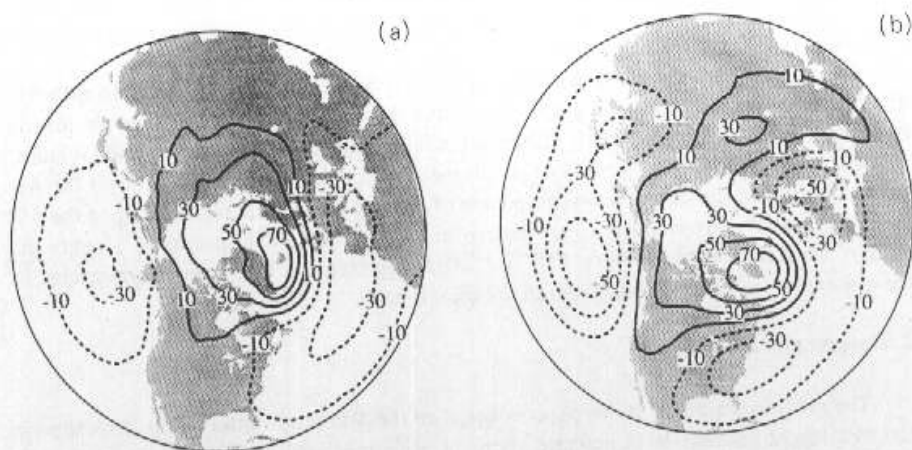


Fig. 1. The modes of two leading EOF's regressing (a) the SLP field and (b) the 500 hPa height field upon the standardized time series of the leading PC's. Contour interval is 20 m; negative contours are dashed.

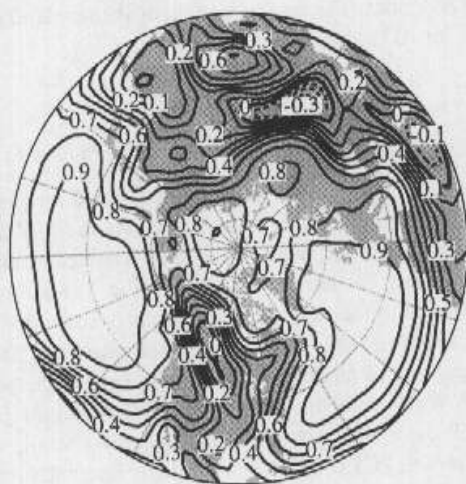


Fig. 2. The correlation coefficients field between the SLP and 500 hPa. Contour Interval is 0.1; negative contours are dashed.

Despite the familiarity of these patterns and the strong correlation between their respective PC time series, the EOF's of the 500 hPa height are much less robust than their SLP counterparts. Using the Monte Carlo procedure, Fig. 3 illustrates the distinction between the EOF's of the 500 hPa height and SLP. The Monte Carlo procedure can be described as follows: The two leading principal component time series based on the entire 119 months record

(hereafter denoted PC1 and PC2) are used as reference time series. EOF analysis is performed on a large number of randomly selected subsets derived from the 119-month dataset. In this case, 60 months were randomly chosen by the 119 months, and 50 times were done, so we have 50 sixty-month subsamples as subsets. The PC's for each subsample are correlated with the counterpart in reference PC1 and PC2, and the resulting pairs of the values are plotted in a Cartesian format: subsample PC1 with reference PC1 as the abscissa, and subsample PC1 with reference PC2 as the ordinate, the point as the asterisk. In all cases, the signs of subsample PC time series are chosen so as to make them positively correlated with the corresponding reference PC' time series.

At 500 hPa, the asterisk points for the individual subsamples tend to be stretched out in thin arcs (Fig. 3a), but in the SLP, the asterisks close to the abscissa equal 1 (Fig. 3b). The results show the concerning robustness of the PC1 in SLP (i.e., AO index). It is evident that the EOF's in the SLP are much more reproducible than the EOF's at 500 hPa height.

### 3.2 Comparison between the meridional structure and stationary wave of $U_t$ and AO index

In this section, the meridional structure and stationary wave signature of the mode of variability described by Ting et al. (1996) and counterpart for the AO index were compared.

The algebraic difference of the zonal-mean geostrophic wind between  $55^\circ\text{N}$  and  $35^\circ\text{N}$  was defined as  $U_t$  index by Ting et al. (1996). The temporal correlation coefficient between  $U_t$  and AO index is 0.85 based on 119-month data, and 0.88 based on 40-season data. The zonal-mean value of 500 hPa and zonal-mean geostrophic wind at 500 hPa are labeled as  $[Z_{500}]$  and  $[U_g]$ , which are functions of latitude.

The meridional profiles of zonal-mean wind amplitude associated with the AO and  $U_t$  index were shown in Fig. 4. They were obtained by regressing the zonal-mean geostrophic wind  $[U_g]$  for each month upon the standardized time series of the two indices. The profile for

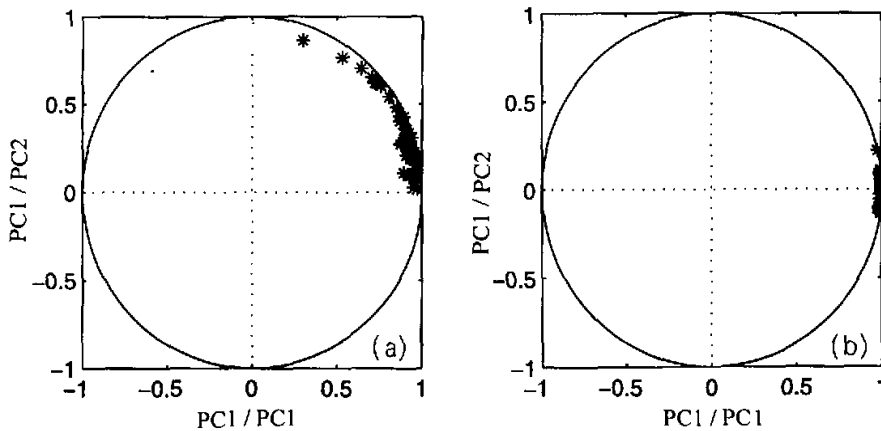


Fig. 3. Projection of two leading perturbed EOF's based on randomly selected 50 sixty month subsamples derived from the 119 original dataset of (a) 500 hPa height, (b) SLP. The correlation coefficients between subsample PC1 and reference PC1 as the abscissa, the subsample PC1 with reference PC2 as the ordinate. The resulting pairs are plotted by asterisks.

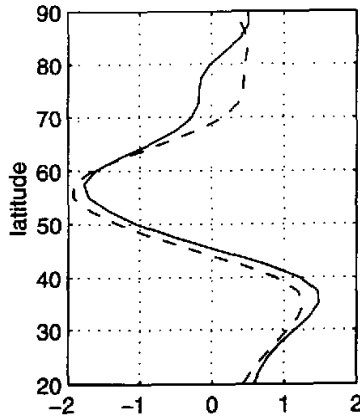


Fig. 4. Zonal-mean wind at 500 hPa level regressed upon Dec-Feb monthly mean values of the AO index (solid line) and Ut index (dashed line).

the Ut index is identical with profile of the Fig. 3 of Ting et al. (1996), the maximum and minimum are located near  $35^{\circ}\text{N}$  and  $55^{\circ}\text{N}$ . The two profiles are very similar; both with respect to amplitude, but the placement of the maximum and minimum for the AO index is shifted northward by  $3^{\circ}$ – $4^{\circ}$  latitude.

In order to compare the patterns of stationary wave induced by the Ut and AO index, we use the station wave component of 500 hPa height field, labeled as  $Z_{500}^*$ . The  $Z_{500}^*$  is that total minus the zonal mean of 500 hPa, it is  $Z_{500}^* = Z_{500} - [Z_{500}]$ .

The corresponding distributions for the  $Z_{500}^*$  regressed on AO and Ut index were shown in Fig. 5. There is a one-to-one correspondence between all the major centers of action in the two maps, especially in the North Atlantic and Eurasian continent. The only discernible difference in two maps is that the features over the Atlantic are slightly stronger in the AO pattern, whereas the features over the Pacific are stronger in the pattern derived from the Ut index.

In order to determine the relationship between the meridional profiles of zonal-mean wind amplitude identified by Ting et al. (1996) and the eddy component at the  $Z_{500}^*$ , we performed singular value decomposition (SVD) analysis upon the  $Z_{500}^*$  field paired with the meridional profile of zonal-mean geostrophic wind at 500 hPa ( $[U_g]$ ), both for the region poleward of  $20^{\circ}\text{N}$  and both weighted by the square root of cosine of latitude. Figure 6 shows the  $[U_g]$  regressed upon the standardized expansion coefficient of the  $Z_{500}^*$  field (Fig. 6b) and the  $Z_{500}^*$  field regressed upon the standardized expansion coefficient of the  $[U_g]$  (Fig. 6a) for the leading mode in this expansion, which accounts for 68% of the squared covariance fraction (SCF1), compared to 22% for the second mode. The expansion coefficient time series are correlated with one another at a level of 0.69. Based on season data, the SCF1 accounts for 71% and the correlation coefficient is 0.84. In Fig. 6a, the pattern is similar to the pattern in

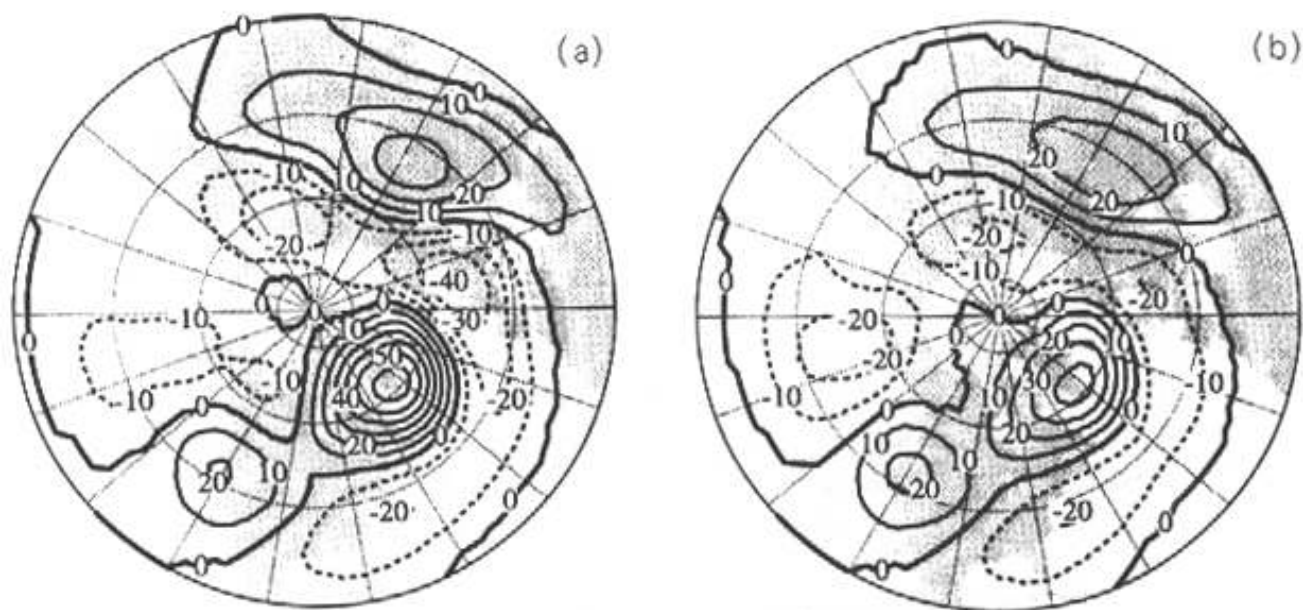


Fig. 5. The eddy component of the 500 hPa height field at the  $Z_{500}^*$  regressed upon (a) DJF monthly mean values of the AO index, and (b) upon the inverted Ut index. Contour interval: 10 m.

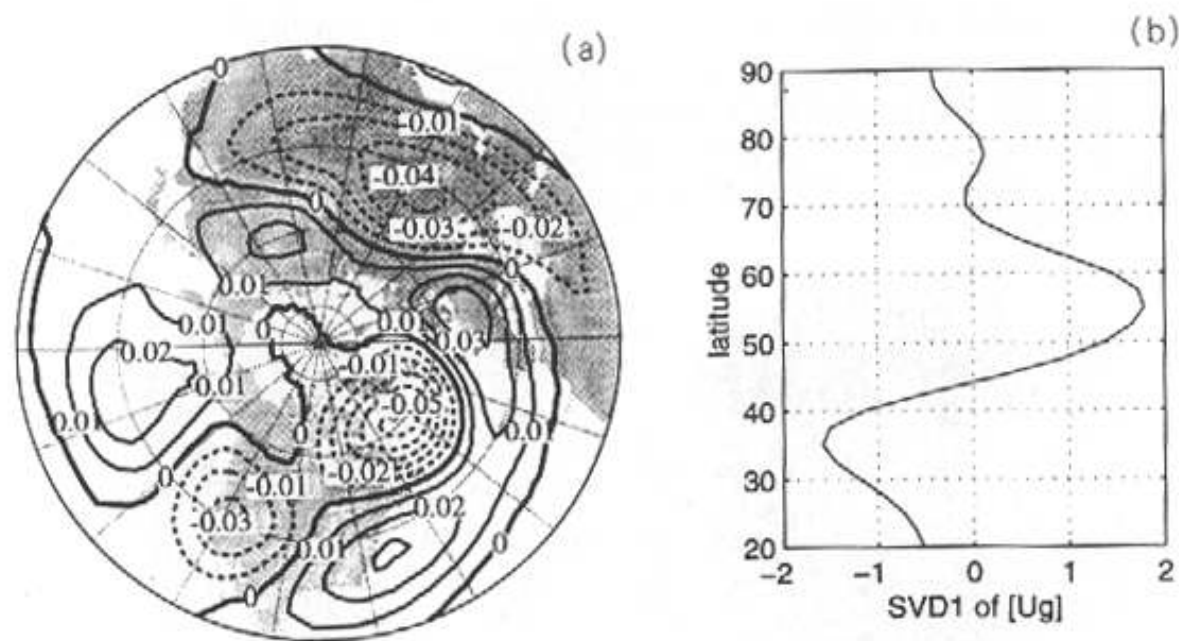


Fig. 6. Heterogeneous regression maps of the leading coupled mode in the  $Z^*$  field and  $[U_g]$  field as determined from SVD analysis. (a) The  $Z_{500}^*$  field, (b) the  $[U_g]$  field. Contour interval is 1000 m.

Figs. 5a and 5b. The major centers of action in the three maps are one-to-one correspondence, especially in the Eurasian continent and North Atlantic. The center values over the area are similar to the pattern derived from AO (Fig. 5a); the prominent patterns of planetary wave variability like the PNA and NAO pattern did not appear. In Fig. 6b, the profile is remarkably similar to the pattern of Ut index in Fig. 4, the AO signature is recognizable in it,

but the relevant features in the zonal wind field are shifted southward by  $3^{\circ}$ – $4^{\circ}$  latitude.

### 3.3 An important pattern — the $Z_{500}^*$ for PC2

It remains to be considered whether there are other important modes of coupling between the zonally averaged flow profile ( $[U_g]$ ) and the stationary waves in the wintertime 500 hPa height field ( $Z_{500}^*$ ). The inherent orthogonality constraints in the SVD analysis render the question why the  $Z_{500}^*$  pattern was corresponded to mutually orthogonal meridional profiles of  $[U_g]$ . Here we choose orthogonal  $Z_{500}^*$  pattern and examine the corresponding  $[U_g]$  profiles, irrespective of whether they are mutually orthogonal from SVD.

As a basis for defining these patterns, we perform empirical orthogonal functions (EOF) analysis on the unstandardized  $Z_{500}^*$  anomaly field. The structure of  $Z_{500}^*$  field regressed upon the two leading standardized principal components PC1 and PC2 was shown in Fig. 7, account for 18% and 14% of the total variance of the  $Z_{500}^*$  field in monthly data, 24% and 18% for season.

The  $Z_{500}^*$  pattern for PC1 contains elements of the familiar PNA pattern from the North Pacific across the North American into the western Atlantic, together with a second wavetrain extending from the North Atlantic across the northern Europe into the central Russia in Fig. 7a. The results for PC2 resemble the patterns in Fig. 5 and Fig. 6a. It means that the eddy component of 500 hPa height field in Fig. 5 is an intrinsic character in the  $Z_{500}^*$  field.

The profiles of the zonal-mean wind at 500 hPa level ( $[U_g]$ ) regressed upon the PC1 and PC2 of the  $Z_{500}^*$  are shown in Fig. 8. In Fig. 8b, the profile for PC2 of the  $Z_{500}^*$  strongly resembles the AO profile in Fig. 4, with respect to both amplitude and placement of the maximum and minimum. The profile for the PC1 is shown in Fig. 8a, the maximum and minimum

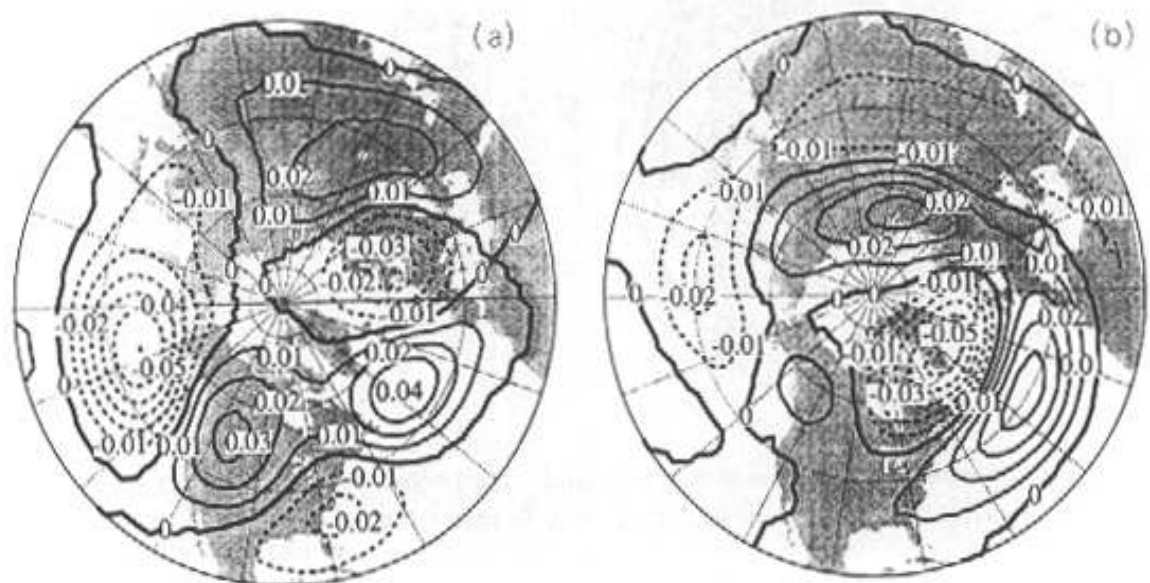


Fig. 7. The modes of the two leading EOF's of wintertime  $Z_{500}^*$  field regressed upon standardized time series of leading PC's: (a) PC1 and (b) PC2. Interval is 1 km.

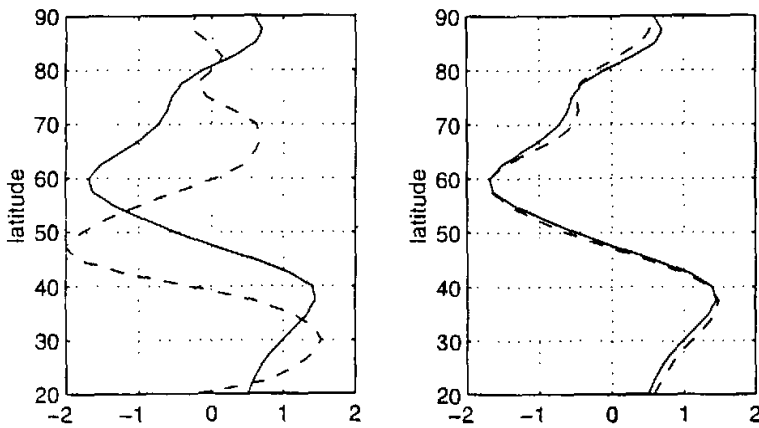


Fig. 8. The profiles of the  $[U_g]$  regressed upon PC1 and PC2 of wintertime  $Z_{500}^*$  field and AO, (a) for PC1 and AO, (b) for PC2 and AO. The solid line is for AO, and the dashed line for PC's.

are located near  $30^\circ\text{N}$  and  $48^\circ\text{N}$ . While it is corresponding with the PNA pattern in Fig. 7a, when the positive polarity  $Z_{500}^*$  with negative  $Z_{500}^*$  anomalies over the North Pacific, the zonally averaged westerly wind tend to be stronger than normal along  $30^\circ\text{N}$  and weaker than normal along  $48^\circ\text{N}$ . The corresponding profiles for PC3, PC4 and PC5 are much weaker (figure omitted).

In order to confirm that there is no other important mode of coupling between the  $Z_{500}^*$  field and the  $[U_g]$  profile, we examined maps of  $Z_{500}^*$  regressed on standardized  $[U_g]$  time series at  $2.5^\circ$  latitude increments ranging from  $20^\circ\text{N}$  to  $87.5^\circ\text{N}$ . Strong patterns that appear to be linear combinations of the ones in Fig. 6a are evident throughout the band extending from  $35^\circ\text{N}$  to  $70^\circ\text{N}$  (figure omitted).

#### 4. Discussion

From the foregoing analysis, it is apparent that a substantial fraction (14% for monthly or 18% for season) of the variance of the Northern Hemisphere wintertime stationary wave field ( $Z_{500}^*$ ) can be specified on the basis of a knowledge of the zonally averaged zonal wind profile  $[U_g]$ . Most of this coupled variability can be represented in terms of two linearly independent coupled data from the  $[U_g]$  and  $Z_{500}^*$ . The coupled modes can be defined in such a way that one closely resembles the mode described by Ting et al. (1996) with opposing peaks in zonal wind profile near  $35^\circ\text{N}$  and  $55^\circ\text{N}$ , and the other has the eddy component of primary peak at intermediate latitudes. The former mode can be interpreted as the "Arctic Oscillation" discussed in the companion paper by Thompson and Wallace (1998, 2000). The corresponding stationary wave patterns contain elements like the "teleconnection patterns", discussed by Wallace and Gutzler (1981), Barnston and Livezey (1987) and others, but they are unlike the prominent teleconnection patterns, they have a hemispheric extent and cannot be



interpreted in terms of the individual wavetrains.

#### REFERENCES

- Branstator, G.W., 1984: The relationship between the zonal-mean flow and quasi-stationary waves in the mid troposphere. *J. Atmos. Sci.*, **41**, 2163–2178.
- Barnston, A., and R.E. Livezey, 1987: Classification, seasonality and persistence of low-frequency circulation patterns. *Mon. Wea. Rev.*, **115**, 1083–1126.
- Cheng, X., G. Nitsche, and J.M. Wallace, 1995: Robustness of low-frequency circulation pattern derived from EOF and rotated EOF analyses. *J. Climatol.*, **8**, 1709–1713.
- Kidson, J. W., 1985: Index cycles in the Northern Hemisphere during the Global Weather Experiment. *Mon. Wea. Rev.*, **113**, 607–623.
- Ting, M., M.P. Hoerling, T. Xu, and A. Kumara, 1996: Northern Hemisphere teleconnection patterns during extreme phases of the zonal-mean circulation. *J. Climate*, **9**, 2615–2633.
- Thompson D. W. J., and J.M. Wallace, 1998: The Arctic oscillation signature in wintertime geopotential height and temperature fields. *Geophys. Res. Lett.*, **25**, 1297–1300.
- Thompson D. W. J., and J.M. Wallace, 2000: Annular modes in the extratropical circulation. Part I: month-to-month variability. *J. Climate*, **13**, 1000–1016.
- Wallace, J. M., and D. S. Gutzler, 1981: Teleconnections in the geopotential height field during Northern Hemisphere winter. *Mon. Wea. Rev.*, **109**, 784–812.

## 500 hPa 场的纬向平均地转风的经向廓线分布 与稳定波型的联系

方之芳

摘 要

应用蒙特卡罗方法、奇异值分解(SVD)、自然正交分解(EOF)和回归分析等统计方法,探讨冬季北半球海平面气压场与500 hPa高度场、500 hPa纬向平均场和纬偏场( $Z_{500}^*$ )中稳定波的联系。依据正交分解分析,海平面气压场的第一与第二特征向量权重之比远大于500 hPa,其比值达2倍,而且它的第一特征场更具有纬向对称性。在应用蒙特卡罗方法讨论上述两场的第一与第二特征向量时间序列的差异时,海平面气压场第一特征向量是十分稳定的,不因随机抽样而改变,一再重复出现;因此认为海平面气压场的第一特征向量场比500 hPa高度场具有更好的重复性和代表性。在比较海平面气压场第一特征向量时间序列(即北冰洋涛动指数)与500 hPa场上 $35^{\circ}\text{N}$ – $55^{\circ}\text{N}$ 纬向风差值(即Ut指数)时,两者的相关达0.85;在它们与500 hPa纬向平均风场的回归廓线图中,无论在振幅和极大极小值的位置上,都十分相似。在比较上述两指数与纬偏场( $Z_{500}^*$ )的回归场时,所有的正负大值中心,位置全部一一对应,中心值也相近,尤其在北大西洋和欧亚大陆。在500 hPa纬向平均风场和纬偏场( $Z_{500}^*$ )的奇异值分解分析中,其结果正与上述两回归场相仿;应用正交分解分析 $Z_{500}^*$ 场,其第二特征向量场与上述的回归场也完全一致。因此认为这种覆盖整个大西洋和欧亚大陆的大气分布型不同于以往常见的遥相关型中的波列结构,而是另一种重要的稳定波型。

关键词: 经向廓线, 稳定波, 涡旋分量, 纬向平均地转风, 北冰洋涛动